Electronic Supplementary Information

Water as Hole-Predatory Instrumental to Create Metal Nanoparticles on Triple-Conducting Oxides

Jun Hyuk Kim[a], Jaewoon Hong[b], Dae-Kwang Lim[a], Sejong Ahn[a], Jinwook Kim[a], Jun Kyu Kim[a], Donghwan Oh[a], SungHyun Jeon[a], Sun-Ju Song[b,*] and WooChul Jung[a,*]

[a] Department of Materials Science and Engineering, KAIST, Daejeon, Republic of Korea

[b] Department of Materials Science and Engineering, Chonnam National University, 77 Yongbong-ro, Buk-gu, 500-757, Gwangju, Republic of Korea

[*]e-mail : song@chonnam.ac.kr, wcjung@kaist.ac.kr

Experimental Procedures

Material fabrication

$BaCo_{0.4}Fe_{0.4}Zr_{0.1}Y_{0.1}O_{3-\delta}$ (BCFZY), $Ba_{0.95}Ag_{0.05}Co_{0.4}Fe_{0.4}Zr_{0.1}Y_{0.1}O_{3-\delta}$ (BCFZY-Ag) powders were synthesized by a sol-gel method. Stoichiometric amounts of barium nitrate ($Ba(NO_3)_2$, Alfa Aesar), cobalt nitrate hexahydrate ($Co(NO_3)_2 \cdot 6H_2O$, Alfa Aesar), iron nitrate nonahydate ($Fe(NO_3)_3 \cdot 9H_2O$, Sigma Aldrich), zirconyl nitrate solution (35 wt.% of $ZrO(NO_3)_2$ in nitric acid, Sigma Aldrich), yttrium nitrate hexahydrate ($Y(NO_3)_3 \cdot 6H_2O$, Sigma Aldrich), and silver nitrate ($AgNO_3$, Sigma Aldrich) were dissolved in D.I. water. For complexing agents, citric acid and Ethylenediaminetetraacetic acid (EDTA) were used, and the molar ratio was 2:1:1 for citric acid, EDTA, and total metal ions. Thereafter, $NH_3 \cdot H_2O$ are added to adjust the pH value to ~9. The solution is then heated at 80^{o}C with vigorous mixing with stir bar. The subsequent evaporation of water results in a dark purple gel, and the gel was pre-fired in heating mantle for 450^{o}C for 3 hours. The resulting pre-calcined powders are consequently calcined at 1000^{o}C for 5 hours to obtain perovskite phase.

Fabrication of symmetric cell and single cells

Symmetric cells (electrode|SDC|electrode) was devised to evaluate the area specific resistance of the developed cathode materials. First, the $BaZr_{0.1}Ce_{0.7}Y_{0.1}Yb_{0.1}$ (BZCYYb) powders (Fuelcellmaterials) containing 1 wt% NiO were dry-pressed in a square steel die and sintered at 1450^{o}C for five hours to form a dense electrolyte pellet. To make a cathode ink slurry, respective electrode powders were ball-milled with ink vehicle (Fuelcellmaterials) with a weight ratio of 1:1 for 24 hours. To facilitate the ball-milling,

extra ethanol was added to the slurry, however later evaporated in an 80^{o}C for overnight. The slurry is then screen-printed on both side of BZCYYb pellet, which is then fired at 900^{o}C for 2 hours to complete the symmetric cell fabrication. Silver paste was used as a current collector.

To demonstrate the single-cell performance, a button cell of Ni-BZCYYb (anode support)|Ni-BZCYYb (anode functional layer, AFL)|BZCYYb (electrolyte)|BCFZY-Ag (O_2-electrode) configurations is used. To prepare the anode support, NiO in powder form (Fuelcellmaterials), BZCYYb (Kceracell company) is ball-milled at a 6:4 weight ratio in ethanol media with toluene (Junsei), fish oil (Sigma Aldrich), poly vinyl butyral (PVB79, Victorchem) and butyl benzyl phthalate (BBP-S160, Victorchem) for 48 hours. The solution is then tape-casted to make the anode support. The anode tape is subsequently dip-coated in an anode functional layer slurry (NiO (Kceracell AFL grade, SSA: ~12 m^2/g) and BZCYYb (Kceracell, SSA: ~12 m^2/g) at a weight ratio of 6:4) suspended in an organic mixture of ethanol, Binder-58 (Kceracell), poly vinyl butyral (PVB79, Victorchem) and butyl benzyl phthalate (BBP-S160, Victorchem). The tape is again dip-coated with the electrolyte suspension and subsequently sintered at 1400^{o}C. Finally, the O_2-electrode paste is screen printed onto the electrolyte side and fired at 1000^{o}C using a microwave furnace (UMF-04, Unicera, Korea). The ramping rate was 50^{o}C/min. The cathode paste is made by mixing the respective powder with a Ferro #441 vehicle at a 1:1 ratio.

Physical Characterizations

The crystal structure of the perovskite phase was confirmed using a high-resolution X-ray diffractometer (X'pert-PRO MRD). To characterize the surface morphology of the water-

mediated ex-solved Ag nanoparticles, SEM (Hitachi S-4800) and TEM (Talos F200X) analyses were performed. To track the oxidation state of Ag before and after the introduction of water vapor, XPS (K-alpha, Thermo VG Scientific) analyses are conducted to investigate the binding energy of Ag3d.

To examine the size and number densities of Ag nanoparticles formed by water vapor, the BCFZY-Ag powder was dry-pressed and corresponding green bodies were sintered at 1150^{o}C for 10 hours to create dense pellets. These pellets were then cleaved to execute water-mediated ex-solution process. Before exposure to water, the samples were annealed under a flowing dry gas in each case (pO_2 = 0.1, 0.21, or 1 atm) at 550^{o}C to reach equilibrium. Then, while maintaining the same level of pO_2, wet gas (pH_2O = 1 vol.%) is flowed by temperature controlled bubbler for 15 minutes.

An experimental apparatus of asymmetric TGA with a Cahn D200 microbalance was used to take the measurements. To prepare the samples, the respective powders are pressed in a square die and subsequently sintered at 1150^{o}C for ten hours to bake dense pellets for the TGA. Before the TGA measurements, the samples were annealed under a flowing dry gas in each case (pO_2 = 0.21 or 1 atm) for 5~15 hours at 600^{o}C to stabilize the weight change fully. After the weight change has equilibrated in the dry gas (i.e., the weight maintains a constant value for one hour within the resolution range (~1ug) of the TGA apparatus), either H_2O or D_2O vapor is flowed at 200 sccm. The pH_2O samples are monitored through a Dewpoint Meter (Model DM70).

Electrochemical Measurements

Electrochemical impedance spectroscopy (EIS) results of the cathode symmetric cell were obtained by AC impedance measurements using a Biologics VSP-300 device as the

workstation (OCV, 1 MHz ~ 0.01 Hz) in the temperature range of 450~650^{o}C. The cells were placed in an alumina tube in contact with a pseudo-four-configuration probe with platinum wire. The mixture gases (O_2-N_2) were flowed into the tube with digital mass flow controllers and bubbler is used to add water vapor.

The typical polarization curves of the single cells were recorded using the Solartron 1287 potentiostat / Solartron FRA analyzer as the workstation in the temperature range of 450~650^{o}C. Current collector of Pt paste (Heraeus 6926) was used. 200 sccm H_2 (3vol.% H_2O) and Air (3vol.% H_2O) are fed into the anode and O_2-electrode respectively during the single cell testing. A.C. impedance was measured at open circuit voltage within the frequency range of 10^6 ~ 10^{-1} Hz (12 points per decade).

To measure electrical conductivity relaxation (ECR), rectangular green bodies of the respective cathode powders (BCFZY, BCFZY-Ag) were initially die-pressed and then sintered at 1150^{o}C for ten hours to create dense bar pellets. ECR is measured using the DC 4 probe method between 450 and 650^{o}C, and pO_2 is switched from 0.21 to 0.1 atm. During the ECR measurement process, pH_2O was maintained at 3 vol%

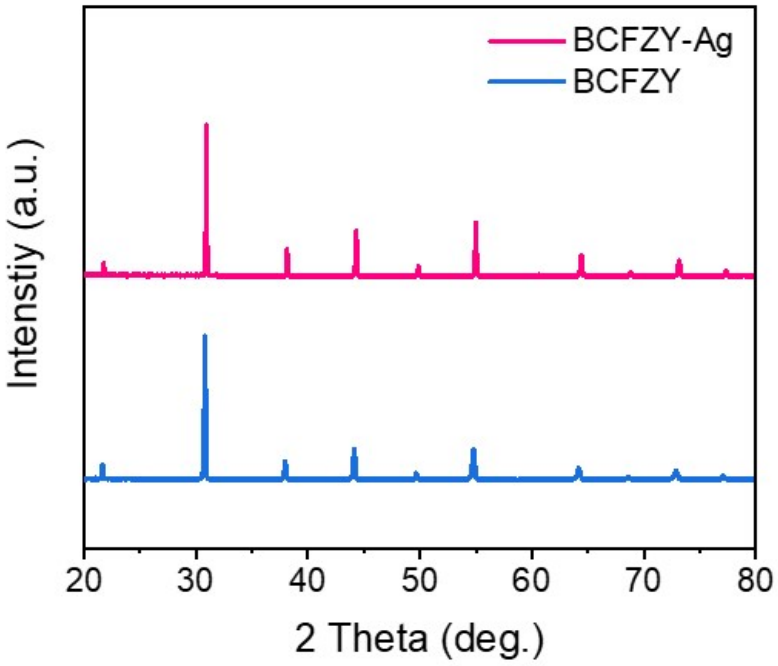

Figure S1. XRD data of the as-synthesized O_2-electrode powders of $BaCo_{0.4}Fe_{0.4}Zr_{0.1}Y_{0.1}O_{3-\delta}$ (BCFZY) and $Ba_{0.95}Ag_{0.05}Co_{0.4}Fe_{0.4}Zr_{0.1}Y_{0.1}O_{3-\delta}$ (BCFZY-Ag).

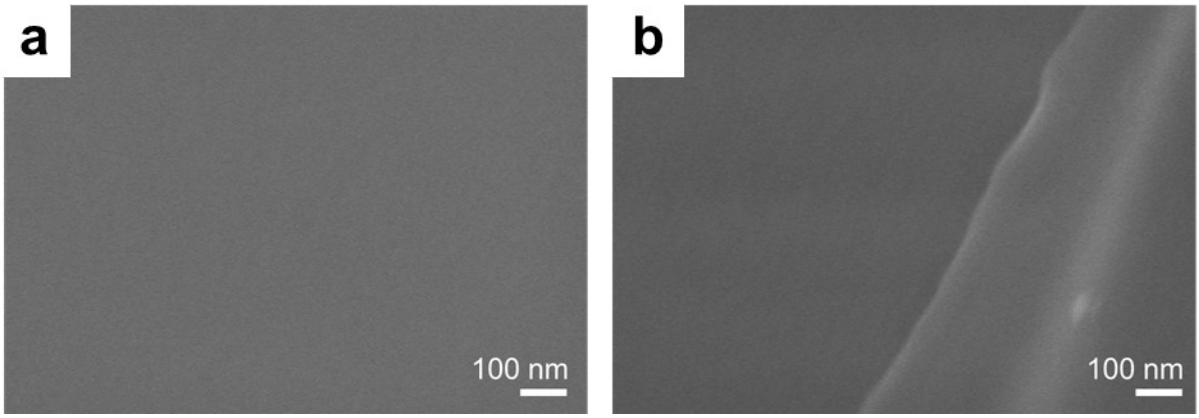

Figure S2. (a), (b) SEM images of BCFZY-Ag pellet surfaces which is heat-treated at 550^{o}C with dry air for > 7 days.

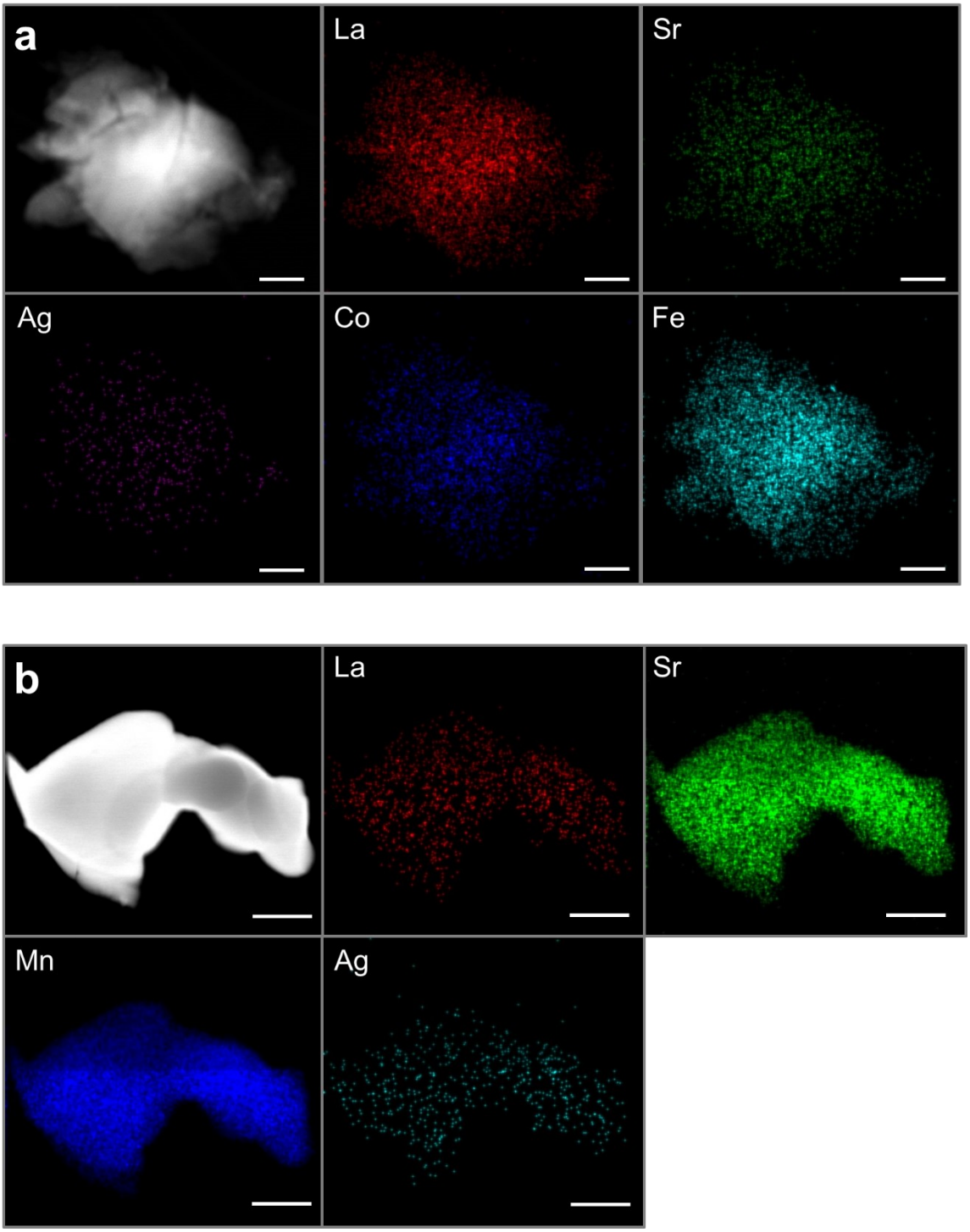

Figure S3. Scanning transmission electron microscopy (STEM) image and electron dispersive X-ray (EDX) results of (a) $(La_{0.6}Sr_{0.4})_{0.95}Ag_{0.05}Co_{0.2}Fe_{0.8}O_{3-\delta}$ (LSCF-Ag) and (b) $(La_{0.8}Sr_{0.2})_{0.95}Ag_{0.05}MnO_3$ (LSM-Ag). Scale bar = 100 nm and 1 μm, respectively.

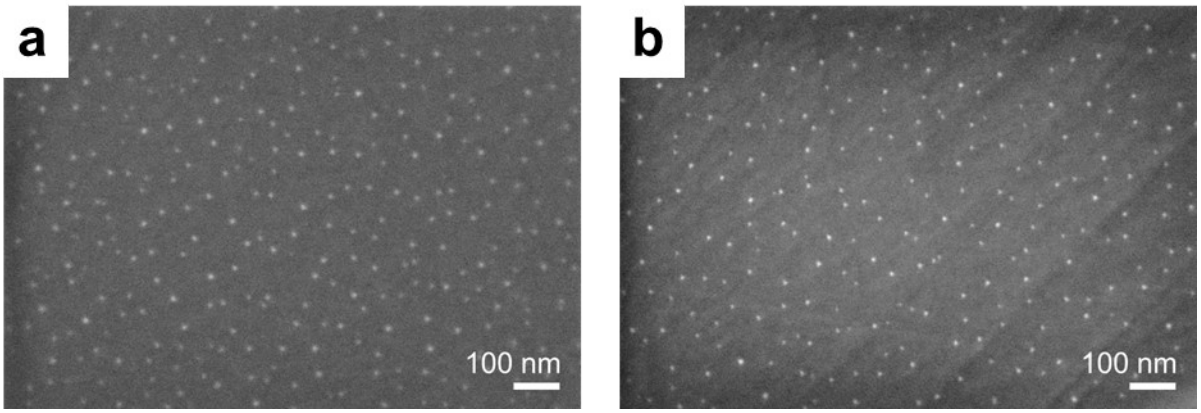

Figure S4. Water-mediated Ag ex-solution from the cleaved bulk surface made by dense pellet of (a) $Ba_{0.95}Ag_{0.05}Co_{0.9}Ta_{0.1}O_{3-\delta}$ (BCT-Ag) and (b) $Ba_{0.95}Ag_{0.05}Co_{0.9}Nb_{0.1}O_{3-\delta}$ (BCN-Ag) after exposure to 3 vol% H_2O/air at 650^{o}C (5 min). (a), (b) illustrated by SEM.

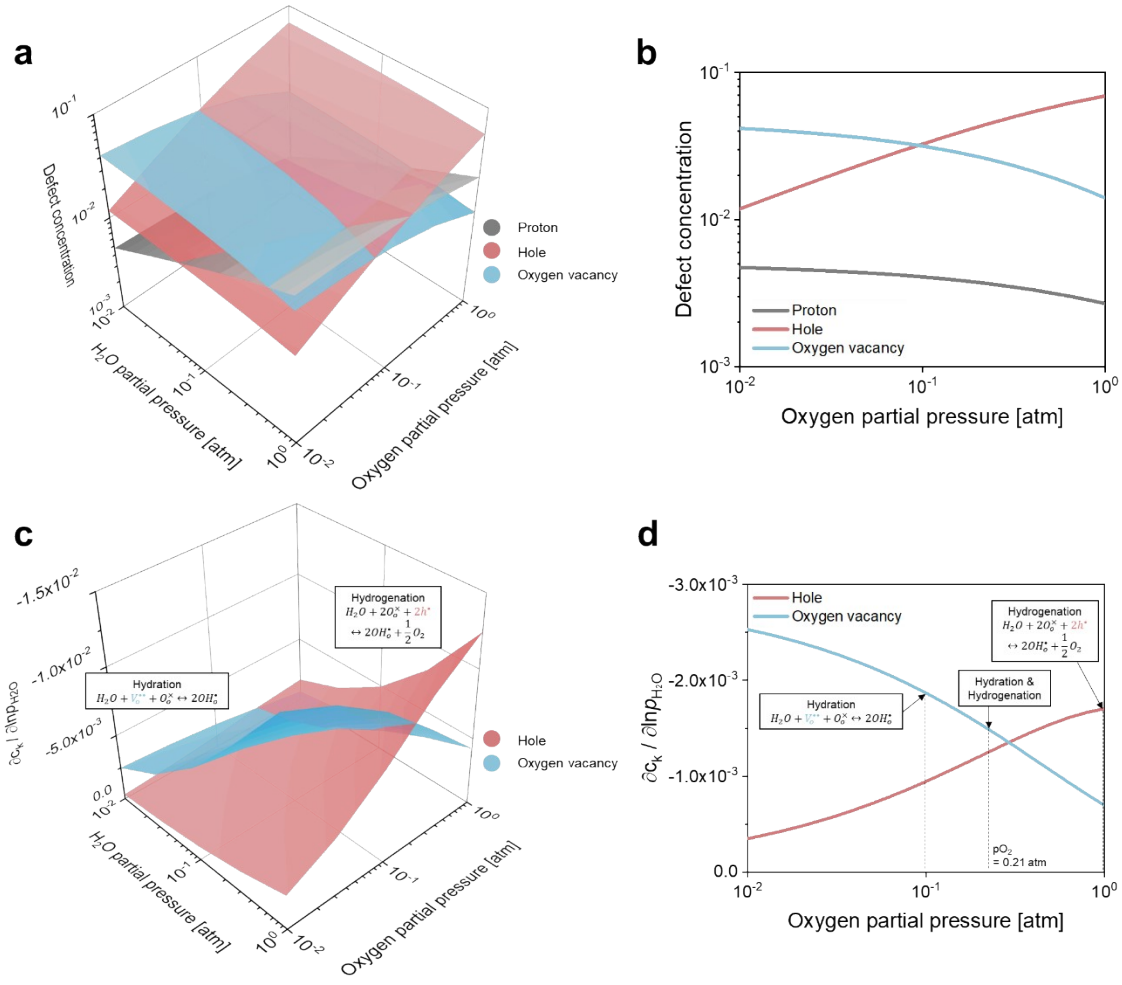

Figure S5. (a) Defect concentrations of proton, hole, and oxygen vacancies in BCFZY-Ag as a function of both the oxygen partial pressure and the H_2O partial pressure at 550°C, (b) Defect concentration of proton, hole, and oxygen vacancies in BCFZY-Ag as a function of oxygen partial pressure at a fixed pH_2O = 0.01 atm at 550°C. (c) Equilibrium response of bulk defect concentrations to changes in pH_2O. The dominating reactions for proton uptake equilibration after pH_2O increase occur mainly due to hydration in the front left section or are caused by hydrogenation in the hind right part. (d) Equilibrium response of bulk defect concentrations to changes in pH_2O (pH_2O = 0.01 atm). With an increase in pO_2, the dominating process shifts from hydration to hydrogenation.

The concentrations of each of the defects in triple-conducting oxides are intercorrelated (i.e., not independent variables; the oxygen site balance is $3 = [O_o^{\times}] + [V_O^{\cdot\cdot}] + [OH_o^{\bullet}]$ and the electroneutrality condition reads $[A^{'}] = 2[V_O^{\cdot\cdot}] + [OH_o^{\bullet}] + [h^{\bullet}]$, where $[A^{'}]$ is the acceptor concentration); hence, the interpretation can be very complex. Simply, under a high pO_2 condition, the defect concentration of holes is ample, while the vacancy and protonic defect concentrations are depleted (Fig. S5b), which subsequently leads to the hydrogenation reaction (Fig. S5d).

The equilibrium of triple-conducting oxides can be expressed by the following equations:

$$\frac{1}{2}O_2 + V_o^{\bullet\bullet} \leftrightarrow O_o^{\times} + 2h^{\bullet}, \quad K_O = \frac{[O_o^{\times}][h^{\bullet}]^2}{pO_2{}^{1/2}[V_O^{\cdot\cdot}]} \text{ (oxygenation, oxidation)}$$

$$H_2O + V_o^{\bullet\bullet} + O_o^{\times} \leftrightarrow 2OH_o^{\bullet}, \quad K_W = \frac{[OH_o^{\bullet}]^2}{pH_2O[O_o^{\times}][V_O^{\cdot\cdot}]} \text{ (hydration)}$$

$$H_2O + 2O_o^{\times} + 2h^{\bullet} \leftrightarrow 2OH_o^{\bullet} + \frac{1}{2}O_2, \quad K_{W/O} = \frac{K_W}{K_O} = \frac{pO_2{}^{1/2}[OH_o^{\bullet}]^2}{pH_2O[O_o^{\times}]^2[h^{\bullet}]^2} \text{ (hydrogenation)}$$

Note that one of the three reactions are redundant ($K_{W/O} = \frac{K_W}{K_O}$). According to the above reactions, the defect concentrations can vary according to the partial pressure of pH_2O and pO_2 and according to the mass actions constants K_o and K_w. Generally, for triple-conducting oxides designed as O_2-electrodes, the Ko value is much higher (orders of magnitude) than $K_{w/o}$ value.[1,2] For example, triple-conducting oxides of $BaCo_{0.4}Fe_{0.4}Zr_{0.2}O_{3-\delta}$ (BCFZ, which is very similar to our composition) shows K_o and $K_{w/o}$ values as ~1 and ~0.006 respectively (at 550°C, pO_2 = 1 bar), indicating that K_o value is ~167 times higher.

By assuming that the mass action constant values of BCFZ are nearly identical to those in our composition, the defect concentration of BCFZY-Ag at 550°C can be devised as shown in Fig. S5a, with the acceptor concentration being $[A^{'}] = 0.1 = [Y_B^{'}]$. We note here that deviations may occur for non-diluted defect concentrations. In the given condition of pH_2O = 0.01 atm, the water vapor partial pressure used for our experimental condition for water-mediated ex-solution, the defect concentrations can be represented as Fig. S5b. As such, at pO_2 > 0.1 atm, the majority of carriers consists of holes, the concentration of which sensitively increases as the pO_2 increases. On the other hand, the concentration of vacancy and protonic defects decrease as the pO_2 increases.

Having identified the individual defect concentrations, the thermodynamic response of a material to changes of pH_2O (at a constant pO_2) can be expressed via the relative change in the respective defect concentration at relative change in pH_2O as follows: $\frac{\partial c_k}{\partial ln(pH_2O)}$

Where ∂c_k denotes a change in respective defect concentration, such as $[V_o^{\bullet\bullet}]\ or\ [h^{\bullet}]$. Fig. S5c illustrates the response regimes to a pH_2O or pO_2 change. For materials with high hole conductivity levels, as in the case of BCFZY-Ag, an increase in the level of pH_2O leads to two scenarios: water uptake through vacancy annihilation (blue area, hydration), or hole consumption (red area, hydrogenation). To be specific, the equilibrium response of defect concentrations ($\frac{\partial c_k}{\partial \ln (pH_2O)}$) at a pH_2O = 0.01atm (where we conducted water-mediated ex-solution) is shown in Fig. S5d. At low pO_2 level of 0.1 atm, the blue line is still higher than hydrogenation line (red) despite the non-negligible hole concentrations, meaning that hydration is the dominant process. At an intermediate pO_2 of 0.21 atm, the contributions to water uptake in hydration and hydrogenation become competitive. Finally, at a high pO_2 of 1 atm, the

equilibrium response regarding hole concentration is predominant, indicating hydrogenation is the governing reaction. It should be emphasized that only hydrogenation can supply the holes required for Ag reduction and thus activate Ag ex-solution. Accordingly, the defect chemistry modeling we present here is consistent with the proposed mechanism of water-mediated ex-solution, and it is confirmed here that changing the pO_2 act as thermodynamic switch to determine the proton incorporating path by consuming the vacancies or holes.

The ex-solution of Ag mediated by water can be written as:

$$Ag_{Ba}^{'} + \frac{1}{2}H_2O + O_o^{\times} \rightarrow Ag_{ex-sol} + V_{Ba}^{''} + OH_o^{\bullet} + \frac{1}{4}O_2 \qquad \text{(Equation S1)}$$

The equilibrium constant for above equation is given by

$$K_{ex-sol} = \frac{a_{Ag}[V_{Ba}^{''}]\left[OH_o^{\bullet}\right](pO_2)^{1/4}}{\left[Ag_{Ba}^{'}\right][O_o^{\times}](pH_2O)^{1/2}} \qquad \text{(Equation S2)}$$

Here, a_{Ag} is the activity of pure Ag, which equals 1. We could also envelop the pO_2 and pH_2O in the equations above using hydrogenation reaction equilibrium constant, $K_{W/O} = \frac{K_W}{K_O} = \frac{{pO_2}^{1/2}\left[OH_o^{\bullet}\right]^2}{pH_2O[O_o^{\times}]^2[h^{\bullet}]^2}$, which conveniently describes the dominating process in various materials and conditions. The substitution of $K_{W/O}$ into Equation S2 yields

$$K_{ex-sol} = \frac{[V_{Ba}^{''}]}{\left[Ag_{Ba}^{'}\right]}(K_{W/O})^{1/2}[h^{\bullet}] \qquad \text{(Equation S3)}$$

The Equation S3 implies that water-mediated ex-solution is half-order proportional to the hydrogenation reaction equilibrium constants, and yields easier at a large electronic defect concentration, as observed in our SEM investigation (for example at a high pO_2 condition such

as $2[V_{\ddot{O}}] < [h^{\bullet}]$). Such an assumption is viable as BCFZY is a majority hole conductor, as total conductivity of the materials is dominated by the hole conductivity.[3]

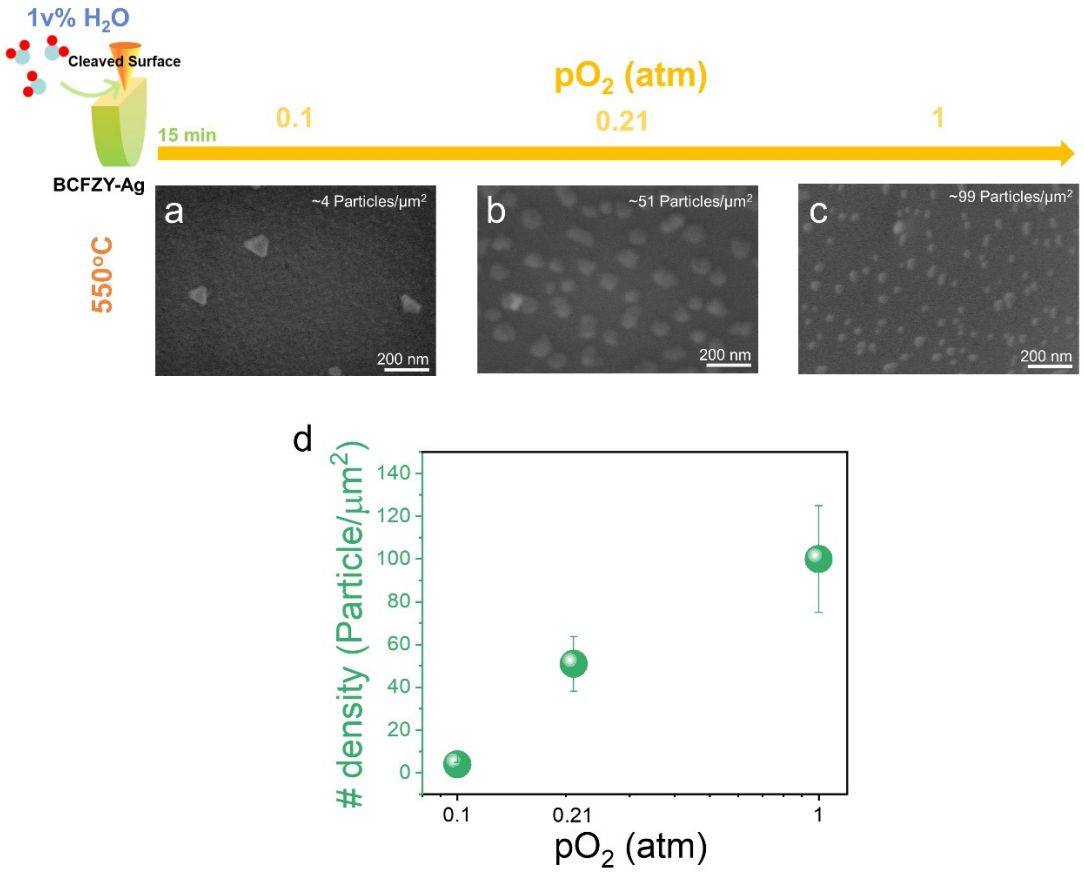

Figure S6. Controlled number densities of Ag nano-catalysts self-assembled on a BCFZY-Ag cleaved surface under oxygen partial pressure (pO_2). (a-c) Scanning electron microscope (SEM) images of the BCFZY-Ag cleaved surface in relation to pO_2 (550°C, pH_2O = 1 vol.%). (d) Quantitative analyses results of water-mediated ex-solved nanoparticles: number density (# density, particle/μm^2) of the nanoparticles depending on the pO_2.

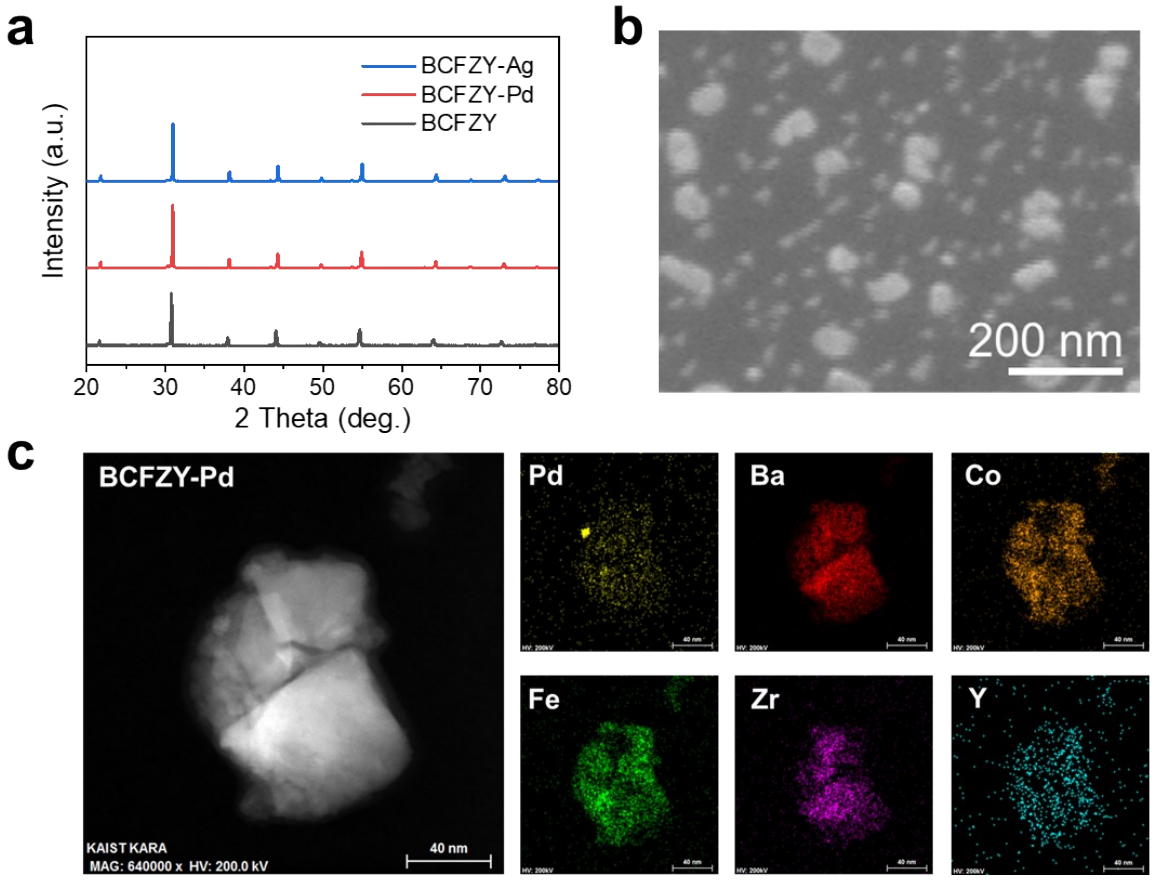

Figure S7. (a) XRD data of the as-synthesized powders of $BaCo_{0.4}Fe_{0.4}Zr_{0.1}Y_{0.1}Pd_{0.05}O_{3-\delta}$ (BCFZY-Pd) compared to BCFZY and BCFZY-Ag, (b) SEM images of the BCFZY-Pd dense pellets after heat treatment in 1 vol% H_2O/air at 650°C, (c) scanning transmission electron microscopy (STEM) image and electron dispersive X-ray (EDX) results.

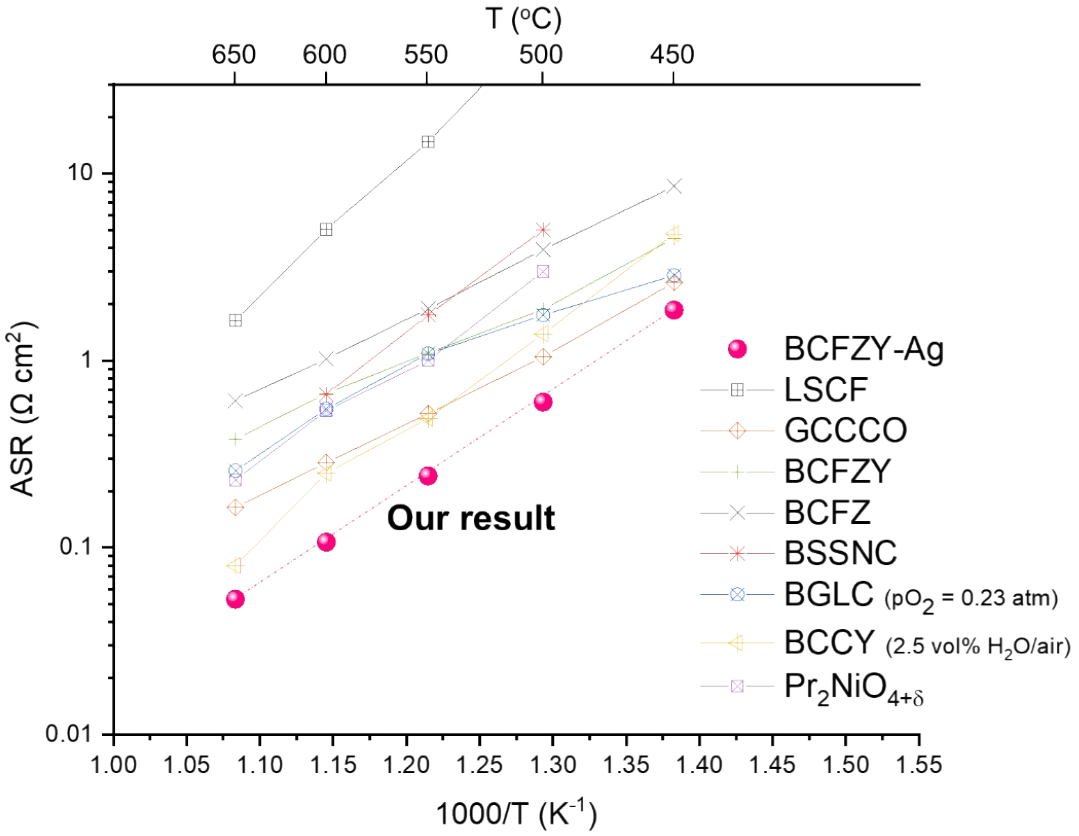

Figure S8. Performance mapping of the ORR performance of the developed BCFZY-Ag O_2-electrode over several benchmark materials.[3-8] (LSCF: $La_{0.6}Sr_{0.4}Co_{0.2}Fe_{0.8}O_{3-\delta}$,[4] GCCCO: $Gd_{0.3}Ca_{2.7}Co_{3.82}Cu_{0.18}O_{9-\delta}$,[9] BCFZY: $BaCo_{0.4}Fe_{0.4}Zr_{0.1}Y_{0.1}O_{3-\delta}$,[3] BCFZ: $BaCo_{0.4}Fe_{0.4}Zr_{0.2}O_{3-\delta}$,[4] BSSNC: $Ba_{0.5}Sr_{0.5}Sc_{0.175}Nb_{0.025}Co_{0.8}O_{3-\delta}$,[10] BGLC: $BaGd_{0.8}La_{0.2}Co_2O_{6-\delta}$ (pO_2 = 0.23 atm),[6] BCCY: $BaCo_{0.7}(Ce_{0.8}Y_{0.2})_{0.3}O_{3-\delta}$ (2.5 vol% H_2O/air),[7] $Pr_2NiO_{4+\delta}$ [8])

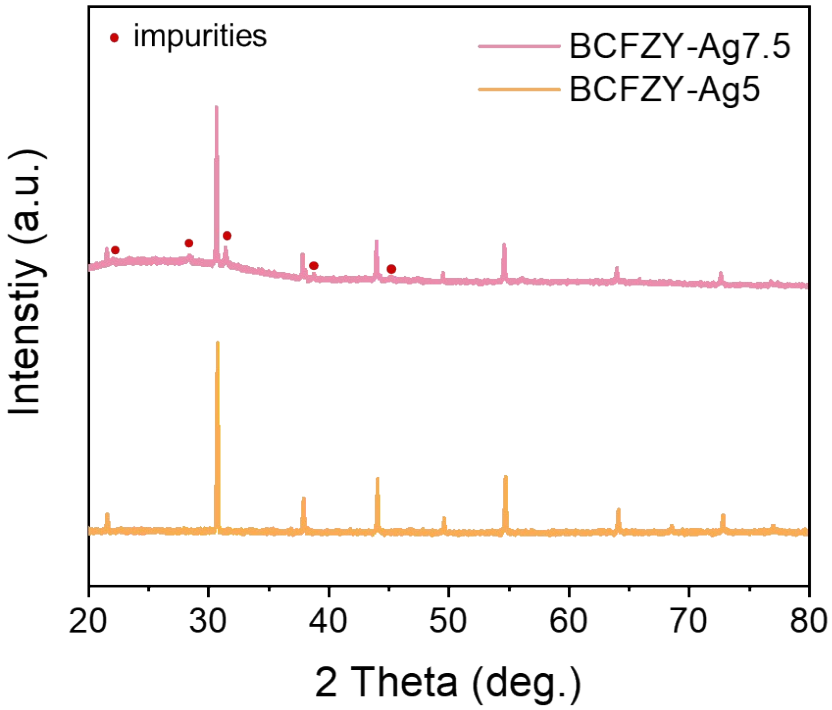

Figure S9. XRD data of the BCFZY-Ag5 and BCFZY-Ag7.5 after 3vol% H_2O exposure (pO_2 = 0.21 atm) at 650°C.

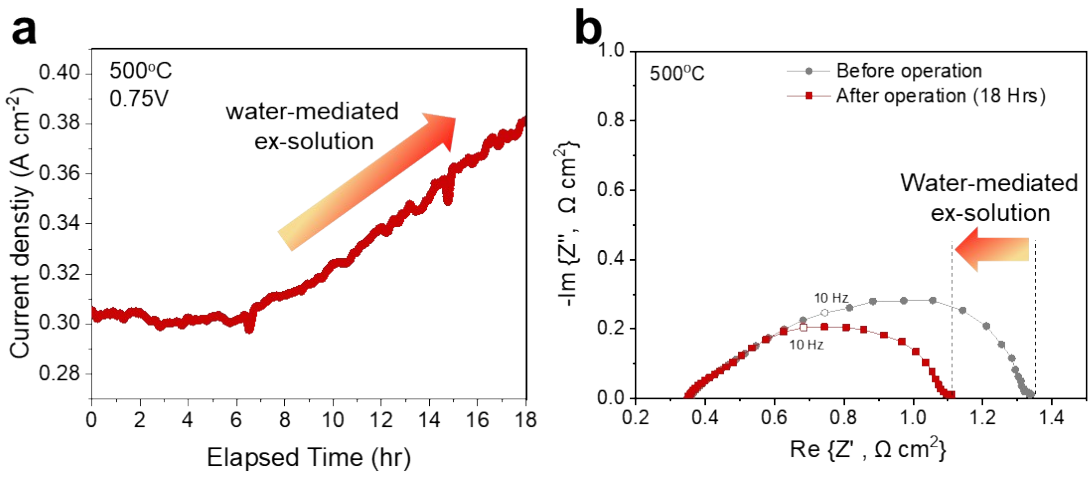

Figure S10. (a) Change in the power density of the BCFZY-Ag based button cell (Ni-BZCYYb | BZCYYb | BCFZY-Ag) under constant operated in dry air (0.75V at 500°C) (b) Corresponding impedance spectra measured under open-circuit voltage before and after operation.

We tested a single PCFC at the initial stage of ex-solution and then tested its performance after a period of time. Please note that the cell was operated in **dry air**, and water vapor is produced in the O_2-electrode during the operation of the fuel cell. The electrochemical testing result are shown in Figure S8. As such, we confirmed the *in situ* activation of the performance of the single cell while constantly operating the cell (~500°C, at 0.75V), as the water that formed at the cathode instantaneously caused the Ag^+ to precipitate into Ag nanoparticles, which act as a catalytic core to boost the ORR rates (Fig. S8a). To examine in detail the cause of this enhancement, we undertook electrochemical impedance spectroscopy measurements in an open-circuit condition (Fig. S8b). Notably, the size of the arc was significantly reduced during the operation (From 0.988 Ω cm^2 to 0.762 Ω cm^2), indicating that Ag was *in situ* ex-solved during operation to reduce the cathode polarization losses.

Table S1. Performance Comparison with Recent PCFCs

Cathode material	Electrolyte	Temperature (°C)	Peak power density (W cm^{-2})	Ref.
BCFZY-Ag	BZCYYb	650	1.20	This work
$BaCo_{0.7}(Ce_{0.8}Y_{0.2})_{0.3}O_{3-\delta}$	BZCYYb	650	0.985	[7]
$PrBa_{0.5}Sr_{0.5}Co_{1.5}Fe_{0.5}O_{5+\delta}$ (without PLD)	$BaZr_{0.4}Ce_{0.4}Y_{0.1}Yb_{0.1}O_{3-\delta}$	650	1.17	[11]
$Gd_{0.3}Ca_{2.7}Co_{3.82}Cu_{0.18}O_{9-\delta}$	BZCYYb	650	1.60	[9]
$PrNi_{0.5}Mn_{0.5}O_3$-$BaPrO_3$	BZCYYb	650	0.44	[12]
$La_{0.6}Sr_{0.4}Co_{0.2}Fe_{0.8}O_{3-\delta}$-$BaZr_{0.5}Pr_{0.3}Y_{0.2}O_{3-\delta}$	$BaZr_{0.7}Pr_{0.1}Y_{0.2}O_{3-\delta}$	650	0.125	[13]
BCFZY-Ag	BZCYYb	600	0.78	This work
BCFZY	BZCYYb	600	~0.65	[3]
$Ba_{0.9}Co_{0.4}Fe_{0.4}Zr_{0.1}Y_{0.1}O_{3-\delta}$	$BaZr_{0.1}Ce_{0.7}Y_{0.2}O_{3-\delta}$	600	~0.67	[14]
$Ba(Co_{0.4}Fe_{0.4}Zr_{0.1}Y_{0.1})_{0.95}Ni_{0.05}O_{3-\delta}$	BZCYYb	600	~0.66	[15]
$PrBa_{0.8}Ca_{0.2}Co_2O_{5+\delta}$	BZCYYb	600	1.06	[16]

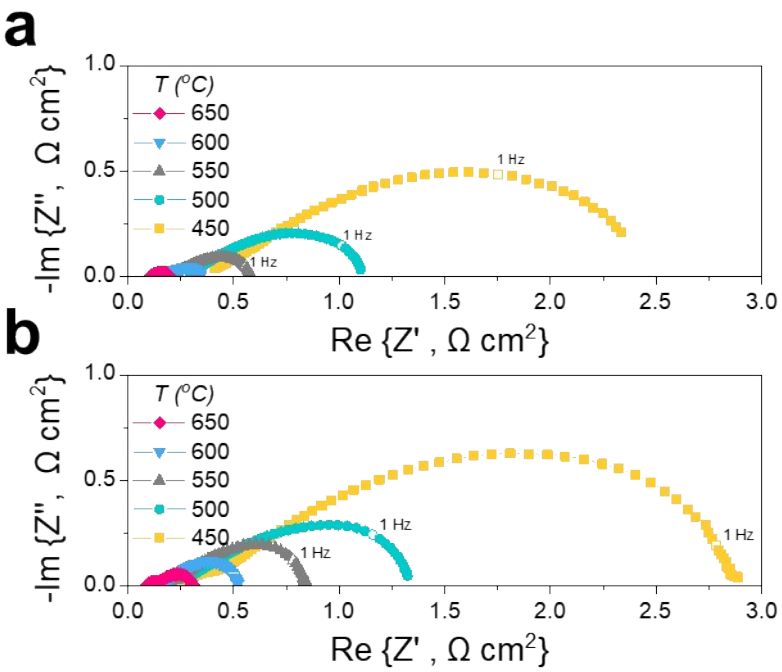

Figure S11. Electrochemical impedance spectroscopy data measured under open circuit voltage for button cells using (a) BCFZY-Ag and (b) BCFZY O_2-electrodes, respectively.

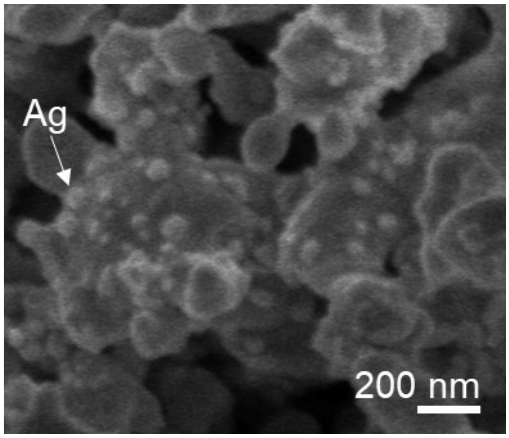

Figure S12. Microstructure of the BCFZY-Ag electrode after ~603 hours of continuous single cell operation at 500°C and thermal cycling.

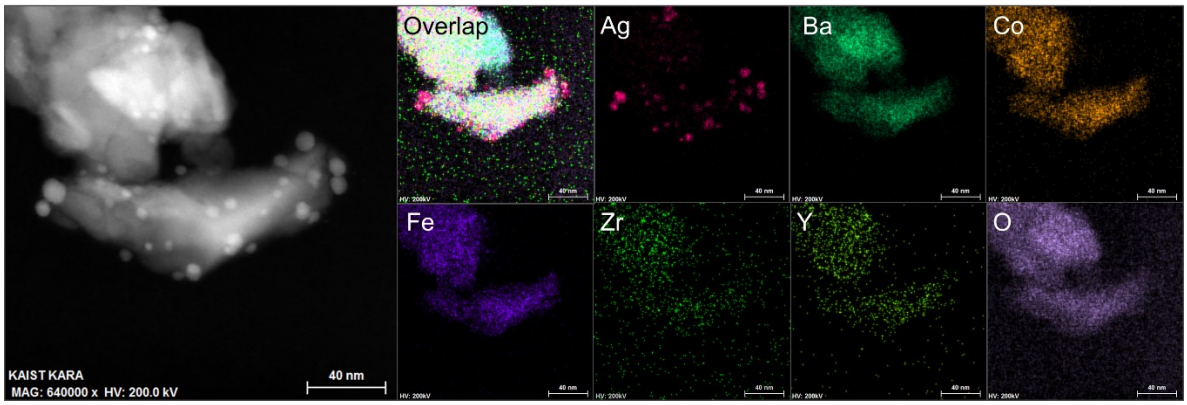

Figure S13. (a) High-angle annular dark-field scanning transmission electron microscopy (HAADF-STEM) image and EDX results of BCFZY-Ag after the long-term stability test under 0.75V operation for ~603 hours at 500^{o}C. Scale bar = 40 nm.

References

1 Poetzsch, D., Merkle, R. & Maier, J. Proton uptake in the H+-SOFC cathode material Ba0. 5Sr0. 5Fe0. 8Zn0. 2O3− δ: Transition from hydration to hydrogenation with increasing oxygen partial pressure. *Faraday discussions* **182**, 129-143 (2015).

2 Zohourian, R., Merkle, R. & Maier, J. Proton uptake into the protonic cathode material BaCo0. 4Fe0. 4Zr0. 2O3-δ and comparison to protonic electrolyte materials. *Solid State Ionics* **299**, 64-69 (2017).

3 Duan, C. *et al.* Readily processed protonic ceramic fuel cells with high performance at low temperatures. *Science* **349**, 1321 (2015).

4 Shang, M., Tong, J. & O'Hayre, R. A promising cathode for intermediate temperature protonic ceramic fuel cells: BaCo 0.4 Fe 0.4 Zr 0.2 O 3− δ. *RSC Advances* **3**, 15769-15775 (2013).

5 Zhang, Y. *et al.* Electrochemical performance and effect of moisture on Ba0.5Sr0.5Sc0.175Nb0.025Co0.8O3-δ oxide as a promising electrode for proton-conducting solid oxide fuel cells. *Applied Energy* **238**, 344-350, doi:https://doi.org/10.1016/j.apenergy.2019.01.094 (2019).

6 Strandbakke, R. *et al.* Gd-and Pr-based double perovskite cobaltites as oxygen electrodes for proton ceramic fuel cells and electrolyser cells. *Solid State Ionics* **278**, 120-132 (2015).

7 Song, Y. *et al.* Self-Assembled Triple-Conducting Nanocomposite as a Superior Protonic Ceramic Fuel Cell Cathode. *Joule* (2019).

8 Grimaud, A. *et al.* Hydration and transport properties of the Pr 2− x Sr x NiO 4+ δ compounds as H+-SOFC cathodes. *Journal of Materials Chemistry* **22**, 16017-16025 (2012).

9 Saqib, M. *et al.* Transition from perovskite to misfit-layered structure materials: a highly oxygen deficient and stable oxygen electrode catalyst. *Energy Environ. Sci.* **14**, 2472-2484 (2021).

10 Zhang, Y. *et al.* Electrochemical performance and effect of moisture on Ba0. 5Sr0. 5Sc0. 175Nb0. 025Co0. 8O3-δ oxide as a promising electrode for proton-conducting solid oxide fuel cells. *Applied Energy* **238**, 344-350 (2019).

11 Choi, S. *et al.* Exceptional power density and stability at intermediate temperatures in protonic ceramic fuel cells. *Nat. Energy*, 1 (2018).

12 Chen, Y. *et al.* An In Situ Formed, Dual-Phase Cathode with a Highly Active Catalyst Coating for Protonic Ceramic Fuel Cells. *Adv. Funct. Mater.* **28**, 1704907, doi:10.1002/adfm.201704907 (2018).

13 Fabbri, E., Bi, L., Pergolesi, D. & Traversa, E. High-performance composite cathodes with tailored mixed conductivity for intermediate temperature solid oxide fuel cells using proton conducting electrolytes. *Energy Environ. Sci.* **4**, 4984-4993 (2011).

14 Ren, R. *et al.* Tuning the defects of the triple conducting oxide BaCo 0.4 Fe 0.4 Zr 0.1 Y 0.1 O 3− δ perovskite toward enhanced cathode activity of protonic ceramic fuel cells. *Journal of Materials Chemistry A* **7**, 18365-18372 (2019).

15 Liang, M. *et al.* Nickel-doped BaCo0. 4Fe0. 4Zr0. 1Y0. 1O3-δ as a new high-performance cathode for both oxygen-ion and proton conducting fuel cells. *Chemical Engineering Journal* **420**, 127717 (2021).

16 Zhou, Y. *et al.* An Active and Robust Air Electrode for Reversible Protonic Ceramic Electrochemical Cells. *ACS Energy Letters* **6**, 1511-1520 (2021).